Application of Information Gap Decision Theory to the Design of Robust Wide-Area Power System Stabilizers Considering Uncertainties of Wind Power

D. P. Ke, F. F. Shen, C. Y. Chung, *Fellow*, *IEEE*, C. Zhang, *Student Member*, *IEEE*, J. Xu, *Member*, *IEEE*, and Y. Z. Sun, *Senior Member*, *IEEE*

***Abstract*--This paper proposes the application of information gap decision theory (IGDT) to the design of robust wide-area power system stabilizers (WPSSs) with consideration of wind farm (WF) power outputs variations and transmission line outages. According to IGDT, an optimization problem is constructed to tune WPSS parameters. Then, the derived optimal WPSSs can achieve explicit and favorable robustness to ensure the required damping control effects on the inter-area oscillations over a maximum variation range of WF steady-state power outputs in normal and emergent operating conditions. Moreover, with the intent of using the excellent global searching capability of particle swarm optimization (PSO), a customized PSO algorithm is proposed to efficiently solve the resulting highly nonlinear programming problem. Finally, simulations are carried out on a modified New England (10-Machine 39-Bus) system to validate the efficiency of the IGDT-based design method. The derived WPSSs exhibit expected robustness with respect to the wind power variations and transmission line outages.**

***Index Terms*--Information gap decision theory, wide-area power system stabilizers, wind power, particle swarm algorithm.**

I. INTRODUCTION

POWER system operation and control are faced with increasing challenges owing to the high penetration of wind power. In particular, wind power integration apparently complicates the small-signal stability in power systems. For example, when doubly-fed induction generators (DFIGs) with primary power control strategies are employed to harness wind resources, their impacts on power system electromechanical oscillations are debatable and depend on several factors, including the location of the wind turbines (WTs), the level of wind power penetration, and so on [1]-[5]. But, recent studies show that DFIG-based WTs can be supplementarily controlled to provide additional damping to power system electromechanical dynamics [6]-[10]. For example, conventional power system stabilizers (PSSs) are installed in DFIGs in [6] and tuned by the phase compensation technique to damp low frequency power oscillations. Moreover, [7] studies the effectiveness of active and reactive power modulations for controlling the modes of electromechanical oscillations. A fairly big focus in this research area has also been placed on the robustness of power system damping control with integration of variable wind power.

Due to the variability nature of wind power, the operating point of a power system can vary within quite a large range. Thus, damping controllers designed for nominal operating points may be unable to suppress inter-area oscillations occurring at other points over this range. Reference [11] attempts to consolidate damping controller robustness by considering different penetration levels of wind power. Analogously, the nominal operating points employed for damping control design are generated in [12] by increasing or decreasing all wind farm (WF) power outputs simultaneously, with the same increments or decrements. Nevertheless, these studies do not explicitly address how to guarantee robust control effects far beyond the nominal operating points. The methodology proposed in [13] could be theoretically regarded as having considered all operating points, i.e., the damping controllers are tuned to optimize the probability distributions of critical eigenvalues. Furthermore, [14] proposes an improved probabilistic method that can more accurately compute the probabilistic eigenvalues for subsequent control design. Although probabilistically robust damping controllers can be synthesized by the above methods, one common premise is that the probability density functions (PDF) of all WF power outputs must be available in advance.

Information gap decision theory (IGDT), developed in the 1980s, is a non-probabilistic and robustness-oriented decision-making theory in uncertain environments [15]. As IGDT can reach the most robust decision with quite low requirements for prior knowledge of the uncertainties, it has received increasing attention in recent years from electric power engineers whose aim is the economical operation of power systems with uncertain renewable energy generations and loads, e.g., optimizing power flow issues of wind-integrated power systems [16], optimizing combinations of supply sources from power markets with uncertain electricity price [17], maximizing generation company profits considering random failures of generators [18], and so on. However, few studies have considered the application of IGDT to power system dynamics control.

This paper is a first attempt to apply IGDT to small signal stability control of power systems. Specifically, wide-area power system stabilizers (WPSSs) are employed to damp the inter-area oscillations of power systems which are impacted by wide operating point drifting due to integration of wind power

This work was supported by the National Natural Science Foundation of China (Grant No.: 51777143). D. P. Ke, F. F. Shen (corresponding author), C. Zhang, J. Xu and Y. Z. Sun are with the School of Electrical Engineering, Wuhan University, Wuhan, Hubei, China (kedeping@whu.edu.cn; shenfeifan@whu.edu.cn). C. Y. Chung is with the Department of Electrical and Computer Engineering, University of Saskatchewan, Saskatoon, Saskatchewan, Canada (c.y.chung@usask.ca).

and risk of losing transmission lines. According to the introduction of IGDT, the design of the WPSSs is based on the solution to a formulated optimization problem with consideration of normal as well as emergent operating conditions (i.e. transmission line outages). Specifically, in each condition, the WPSSs with optimized parameters will maximize the variation region of operating points in which the inter-area oscillations can be satisfactorily suppressed. Thus, compared to H_∞/H_2 norms-based robustness concepts [19], the WPSS robustness in this paper is direct and explicitly understandable, and also enhanced to the highest level by the optimized parameters. Moreover, deriving the robust WPSSs requires little information about the wind power's probability distribution. In particular, a customized particle swarm optimization (PSO) algorithm that preserves the global searching capability of the standard PSO is proposed to solve the above optimization problem in a computationally efficient manner.

The remainder of the paper is organized as follows. Section II introduces IGDT in detail. Section III presents the optimization problem to tune the WPSSs based on IGDT. The customized PSO is depicted in Section IV. Simulations are provided in Section V, and Section VI concludes the paper.

II. Information Gap Decision Theory

IGDT is not a technological theory but a methodology with a domain of relevance, because it focuses on the disparity between what is known and what could be known [15]. One pivotal difference between IGDT and other decision theories is that IGDT models uncertainties based on the information gap, or the interval between the expected (known) value and the actual value, rather than probability. So, IGDT can model uncertainties in cases with a severe lack of information. Moreover, one significant application of IGDT is to help decision makers make robust decisions under uncertain circumstances. Here, robustness denotes the requirements on the system's immunity against uncertainties. So, IGDT proposes a specific function (or index) used for quantitative measurement of the robustness. In this context, uncertainties model and robustness function act as two key components to formulate IGDT-based optimization problem from which robust decision can be derived. Thus, the following subsections will introduce the details of these important IGDT components.

A. System Operation Performance

The function $R(q, u)$ is utilized to represent the operation performance of a system affected by the decision variable q and the uncertain variable u. For instance, $R(q, u)$ could be the damping ratio of an electromechanical mode of concern in a power system. Therefore, the system is considered to be in normal operation when minimal performance requirements (r_c) are satisfied, as follows:

$$\text{Objective: } R(q,u) > r_c \tag{1}$$

$$\begin{cases} H(q,u) = 0 \\ G(q,u) > 0 \end{cases} \tag{2}$$

where $H(\cdot)$ and $G(\cdot)$ are the other equality and inequality constraints of the system's operation, respectively.

B. Uncertainties Model

The uncertain variable can be modeled in several forms by IGDT [15]. In this paper, the following uncertainties model is employed:

$$u \in U(\alpha, \bar{u}) \tag{3}$$

$$U(\alpha, \bar{u}) = \{u : |u - \bar{u}| \le \alpha \bar{u}\}, \alpha > 0 \tag{4}$$

where $\bar{u}$ denotes the predefined expected value of the uncertain variable and α measures the uncertain extent of u. Thus, this model considers that the deviation of u with respect to $\bar{u}$ will not surpass $\alpha\bar{u}$.

C. Robustness Function and Optimal Decision

The robustness function in IGDT is literally described, as follows:

$\alpha_m(q)$ = max {α: *minimal requirements on system operation performance are always satisfied*} (5)

Equation (5) means that the greatest robustness is reached when the system is immune to the maximum degree of uncertainties with simultaneous satisfaction of the minimal requirements with respect to system operation performance. Moreover, the robustness is also dependent on the decision variable (q). Thus, the optimal (robust) decision corresponds to q, which maximizes α_m.

Based on (1)-(5), the robust decision can be derived by solving the following optimization problem:

$$\max_q \quad \alpha \tag{6}$$

$$\begin{cases} H(q,u) = 0 \\ G(q,u) > 0 \\ R(q,u) > r_c \\ \forall\ u \in U(\alpha, \bar{u}), \quad \alpha > 0 \end{cases} \tag{7}$$

The above optimization problem (6)-(7) is concise but clearly delivers the essence of IGDT: first, the robustness measurement (or say, size of the robust region) α makes sense only when all the constraints (representing the minimal requirements on the operational performance of the system) hold for any uncertain variable u in the robust region $U(\alpha,\bar{u})$; then, the optimal decision (solution) q is the one which maximizes α.

Indeed, (6)-(7) is a general and universal optimization which is known as the envelop-bound model in the IGDT family. A number of literatures have shown that the most effective and efficient way of applying IGDT in a specific problem is to map the IGDT components to the concrete objects of this problem [16]-[18]. Then, the optimization solved for the optimal decision can be formulated according to the IGDT model, such as the envelop-bound model. Hence, this paper will follow this procedure to derive an IGDT-based optimization issue which is used to tune wide-area damping controllers.

III. Designing WPSSs Based on IGDT

Uncertainties in WF power outputs in the steady state may influence the small-signal stability of a system by altering the system's power flow. Therefore, a novel method based on IGDT is proposed to design robust WPSSs for suppression of inter-area oscillations in power systems with considerable operating point drifts due to wind power and system parameter changes.

A. *Preliminaries for Design*

The closed-loop structure of a power system is shown in Fig. 1, where the measured signal y is used as input signal of the feedback control system ($K(s)$) which generates the control input signal u_{wpss} to control the power system. The nonlinear model of the closed-loop system can be linearized around an operating point. Hence, the eigenvalues of the state matrix derived from the linearized model indicate the small-signal stability of the system at this point. Specifically, the structure (Fig. 1) of the WPSSs used in this study consists of the traditional phase lead-lag blocks with three tunable parameters (gain K, time constants T_1, T_2) and a washout block with a fixed time constant T_{w}. Above three tunable parameters can markedly influence the electromechanical oscillation modes of concern.

It is assumed that $\mathrm{N_t}$ traditional synchronous generators and $\mathrm{N_w}$ WFs are connected to the system; their steady-state power outputs are represented by $p_{\mathrm{t1}},\ p_{\mathrm{t2}},\ \ldots, p_{\mathrm{tN_t}}$ and $p_{\mathrm{w1}},\ p_{\mathrm{w2}},\ \ldots,\ p_{\mathrm{wN_w}}$, respectively. At a nominal operating point, the WF power outputs are assumed to be the expected values ($\bar{p}_{\mathrm{w1}},\ \bar{p}_{\mathrm{w2}},\ \ldots, \bar{p}_{\mathrm{wN_w}}$). However, as mentioned, the WF practical power outputs in the steady state might deviate from their expected values. Thus, the conventional generators would also change their power outputs from scheduled values at the nominal operating point in order to maintain the generation-load balance of the whole system. This addresses the operating point shift caused by the wind power variation, which consequently affects the small-signal stability (eigenvalues) of the system.

According to the above discussion, the eigenvalues (modes) of the closed-loop system are determined by the WPSS parameters and the WF steady-state power outputs, which can be mathematically expressed as follows:

$$\lambda_i = f_i\left(\boldsymbol{S}, \boldsymbol{X}\right) \qquad i=1, 2, \ldots, \mathrm{N_a} \tag{8}$$

where λ_i denotes the ith interested mode; $\mathrm{N_a}$ is the number of such modes; $f_i(\cdot)$ is a highly nonlinear function; $\boldsymbol{X}$ is the vector consisting of the adjustable parameters of the WPSSs; and $\boldsymbol{S}$ is the vector defined as follows:

$$\boldsymbol{S} = \left[\, p_{\mathrm{w1}}, p_{\mathrm{w2}}, \ldots, p_{\mathrm{wN_w}} \,\right] \tag{9}$$

A large number of approaches to damping power system electromechanical oscillations of inter-area modes are based on properly placing the eigenvalues of closed-loop systems in the complex plane [11]-[13]. Hence, the desired WPSSs ($\boldsymbol{X}$) should consistently work well to meet prespecified placements of all λ_i when the uncertain WPG $\boldsymbol{S}$ varies in a region as large as possible. Obviously, this requirement on designing WPSSs exactly matches the philosophy of IGDT. Therefore, this paper follows the procedure introduced at the end of Section II to apply IGDT for the design of WPSSs. In particular, the concrete IGDT components relevant to this damping control problem are prepared. For example, the requirements on eigenvalue placement represent the minimal system performance requirements. Hence, before constructing the specific optimization problem according to (6)-(7), these IGDT components are introduced first in the following subsections.

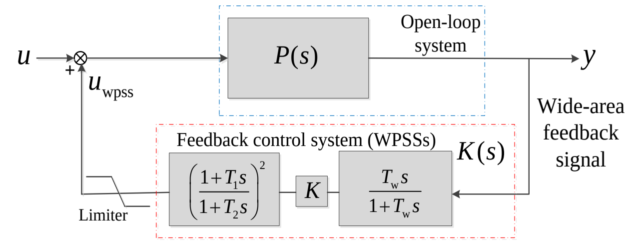

Fig. 1. A closed-loop power system

B. *Requirements on Eigenvalue Placement to Suppress Inter-area Oscillations*

To damp the inter-area oscillations, the most direct objective for eigenvalue placement-based control design is to move the inter-area modes to the region with satisfactory damping in the complex plane. Besides the nominal operating condition, system damping levels under the emergent operating conditions (e.g. transmission line outages) are also considered. Thus, this objective can be expressed in terms of the damping ratio, as follows:

$$\text{Objective: } \xi_i^{(n)} \ge \xi_{i\_\mathrm{spec}}^{(n)} \quad n=1, 2, \ldots, \mathrm{N_s} \text{ and } i=1, 2, \ldots, \mathrm{N_a^{(n)}} \tag{10}$$

where $\mathrm{N_s}$ denotes the number of operating conditions considered during the design of WPSSs; $\mathrm{N_a^{(n)}}$ is the number of the targeted oscillation modes in the nth operating condition and they are successively numbered from 1 to $\mathrm{N_a^{(n)}}$; and ξ is the damping ratio of λ with the following definition:

$$\xi = -\frac{\sigma}{\sqrt{\sigma^2 + \omega^2}} \tag{11}$$

where σ and ω are the real and imaginary parts, respectively, of λ; and $\xi_{i\_\mathrm{spec}}^{(n)}$ is the prespecified acceptable damping ratio of $\lambda_i^{(n)}$.

In addition to the requirements on the damping ratios of the inter-area modes, it is generally preferable that the frequencies of these electromechanical modes be only mildly affected by the damping controllers, because considerable frequency excursion may adversely influence the system transient stability. Thus, the following constraints on frequency changes normally hold for tuning parameters of the damping controllers:

$$\left|\omega_i^{(n)} - \omega_{i\_\mathrm{o}}^{(n)}\right| \Big/ \omega_{i\_\mathrm{o}}^{(n)} \le \rho_i^{(n)} \tag{12}$$

where $\omega_{i\_\mathrm{o}}^{(n)}$ is the frequency of $\lambda_i^{(n)}$ in the open-loop state and $\rho_i^{(n)}$ indicates the allowable frequency changing ratio.

Based on the above introductions, the inter-area oscillations are considered to have been feasibly suppressed by the WPSSs if the following requirements are satisfied:

$$\text{Objective: } \xi_i^{(n)} \ge \xi_{i\_\mathrm{spec}}^{(n)} \tag{13a}$$

$$s.t.\ \left|\omega_i^{(n)} - \omega_{i\_o}^{(n)}\right| / \omega_{i\_o}^{(n)} \le \rho_i^{(n)} \tag{13b}$$

$$n = 1, 2, \ldots, \mathrm{N_s} \text{ and } i = 1, 2, \ldots, \mathrm{N_a^{(n)}} \tag{13c}$$

$$\mathbf{X}_{\min} \le \boldsymbol{X} \le \mathbf{X}_{\max} \tag{13d}$$

Where $\mathbf{X}_{\max}$ and $\mathbf{X}_{\min}$ denote the upper and lower boundaries of $\boldsymbol{X}$, respectively.

C. IGDT-Based Optimization for Tuning WPSS Parameters

Section II described the structure of the robust decision based on IGDT ((3)-(4) and (6)-(7)). By matching (13) to this structure, the robust decision (optimization) of the WPSS parameters mentioned at the end of Subsection III-A can be formulated. In particular, a power system integrated with only two WFs ($\mathrm{N_w}$=2) is taken as an example to demonstrate the optimization problem. So, these two WFs' steady-state power outputs p_{w1} and p_{w2} are two uncertain variables and then handled by the uncertainties model in IGDT. Inspired by (3) and (4), a round region is constructed to depict the possible values (positions) of the two uncertain variables. According to the distribution characteristics of wind power, the operating point (p_{w1}, p_{w2}) corresponding to the two WFs' power outputs is normally with a large probability to appear around the expectation point ($\bar{p}_{\mathrm{w1}}$, $\bar{p}_{\mathrm{w2}}$). Therefore, if a robust round region is constructed and maximized using the expectation point as center, the occurring probability of the event that the required damping control effects are satisfied will be apparently enhanced. Thus, according to above explanations, the uncertainties of wind power generation will be described by a round region, as follows:

$$\left(p_{\mathrm{w1}}, p_{\mathrm{w2}}\right) \in U\left(\bar{p}_{\mathrm{w1}}, \bar{p}_{\mathrm{w2}}, R_{\mathrm{m}}\right) \tag{14}$$

$$U\left(\bar{p}_{\mathrm{w1}}, \bar{p}_{\mathrm{w2}}, R_{\mathrm{m}}\right) = \left\{\left(p_{\mathrm{w1}}, p_{\mathrm{w2}}\right) : \sqrt{\left(p_{\mathrm{w1}} - \bar{p}_{\mathrm{w1}}\right)^2 + \left(p_{\mathrm{w2}} - \bar{p}_{\mathrm{w2}}\right)^2} \le R_{\mathrm{m}}\right\} \tag{15}$$

where R_{m} is the radius of the round region. Then, together with (13), the IGDT-based optimization for deriving the WPSS parameters (robust decision) can be built, as follows:

$$\max_{X}\ R_{\mathrm{s}} = \sum_{n=1}^{\mathrm{N_s}} W^{(n)} R_{\mathrm{m}}^{(n)} \tag{16a}$$

$$s.t.\ \left|\omega_i^{(n)} - \omega_{i\_o}^{(n)}\right| / \omega_{i\_o}^{(n)} \le \rho_i^{(n)} \tag{16b}$$

$$\xi_i^{(n)} \ge \xi_{i\_\mathrm{spec}}^{(n)} \tag{16c}$$

$$\forall\left(p_{\mathrm{w1}}^{(n)}, p_{\mathrm{w2}}^{(n)}\right) \in U\left(\bar{p}_{\mathrm{w1}}^{(n)}, \bar{p}_{\mathrm{w2}}^{(n)}, R_{\mathrm{m}}^{(n)}\right) \tag{16d}$$

$$U\left(\bar{p}_{\mathrm{w1}}^{(n)}, \bar{p}_{\mathrm{w2}}^{(n)}, R_{\mathrm{m}}^{(n)}\right) = \left\{\left(p_{\mathrm{w1}}^{(n)}, p_{\mathrm{w2}}^{(n)}\right) : \sqrt{\left(p_{\mathrm{w1}}^{(n)} - \bar{p}_{\mathrm{w1}}^{(n)}\right)^2 + \left(p_{\mathrm{w2}}^{(n)} - \bar{p}_{\mathrm{w2}}^{(n)}\right)^2} \le R_{\mathrm{m}}^{(n)}\right\} \tag{16e}$$

$$n = 1, 2, \ldots, \mathrm{N_s} \text{ and } i = 1, 2, \ldots, \mathrm{N_a^{(n)}} \tag{16f}$$

$$\mathbf{X}_{\min} \le \boldsymbol{X} \le \mathbf{X}_{\max} \tag{16g}$$

where $R_{\mathrm{m}}^{(n)}$ is the radius of the round region in the nth operating condition; $W^{(n)}$ is the weight to indicate the relative priority of optimizing the performance of WPSSs in the nth operating condition; R_{s} is the weighted sum of $R_{\mathrm{m}}^{(n)}$ with respect to $\mathrm{N_s}$ considered operating conditions; $p_{\mathrm{w1}}^{(n)}$ and $p_{\mathrm{w2}}^{(n)}$ are the power outputs of the two WFs, respectively, in the nth operating condition; $\bar{p}_{\mathrm{w1}}^{(n)}$ and $\bar{p}_{\mathrm{w2}}^{(n)}$ are the expected values of $p_{\mathrm{w1}}^{(n)}$ and $p_{\mathrm{w2}}^{(n)}$, respectively. Highlighted here is that the above formulation procedure of (16) is also suitable for cases with more than two WFs.

So far, the IGDT-based optimization (16) has already been formulated. Specifically, the optimal WPSSs ($\boldsymbol{X}$) solved from (16) can also meet the specified damping control requirements in the considered emergent conditions. This indicates that the optimal WPSSs have favorable robustness not only against the regular wind power variations but also against emergent events such as transmission line outages. In addition, (16) is a highly nonlinear programming problem, and thus a novel method to solve it is proposed in the next section.

IV. Customized Particle Swarm Optimization Algorithm

Particle swarm optimization (PSO) is a self-educating optimization method inspired by bird flocking behavior that has been widely used to solve highly nonlinear optimization problems [20]. Thus, to harness the powerful searching capability of PSO and also avert the prohibitive computational burden, a customized PSO algorithm is proposed to solve the nonlinear programming problem of (16). Briefly, the customized PSO follows the standard PSO procedure but employs additional techniques to significantly relieve the intensity of the computation yet impart limited adverse impacts on the searching quality.

A. Standard PSO Procedure

The general procedure of the standard PSO is briefly outlined as follows:

1) Generate a population including a number ($\mathrm{N_p}$) of particles: $\boldsymbol{X}_k^{(j)}$ and $\boldsymbol{V}_k^{(j)}$ (k=1,2,…,$\mathrm{N_p}$) denote the position and updating velocity, respectively, of the kth particle in the jth iteration. The startup values ($\boldsymbol{X}_k^{(0)}$ and $\boldsymbol{V}_k^{(0)}$) of these terms are randomly produced within prespecified ranges. Here, each particle $\boldsymbol{X}$ denotes a possible solution of (16).

2) Define a fitness function $F(\boldsymbol{X}_k^{(j)})$ to indicate the quality of $\boldsymbol{X}_k^{(j)}$: the larger the fitness function, the better is $\boldsymbol{X}_k^{(j)}$. In this study, $F(\boldsymbol{X}_k^{(j)})$ can be simply selected to be R_{s} in (16a). Accordingly, let $\boldsymbol{P}_k$ be the best position of the kth particle among all positions where it has ever travelled, and let $\boldsymbol{P}_{\mathrm{g}}$ be the best among all $\boldsymbol{P}_k$ (k=1,2,…,$\mathrm{N_p}$).

3) Calculate $\boldsymbol{X}_k^{(j+1)}$ and $\boldsymbol{V}_k^{(j+1)}$ as follows:

$$\begin{cases} \boldsymbol{V}_k^{(j+1)} = e\boldsymbol{V}_k^{(j)} + c_1 r_1\left(\boldsymbol{P}_k - \boldsymbol{X}_k^{(j)}\right) + c_2 r_2\left(\boldsymbol{P}_{\mathrm{g}} - \boldsymbol{X}_k^{(j)}\right) \\ \boldsymbol{X}_k^{(j+1)} = \boldsymbol{X}_k^{(j)} + \boldsymbol{V}_k^{(j+1)} \end{cases} \tag{17}$$

where e is the inertial weight; c_1 and c_2 are the learning factors; and r_1 and r_2 are random numbers between 0 and 1.

4) Evaluate the fitness function for all particles in the j+1 iteration. Compare the current position of the kth particle with $\boldsymbol{P}_k$, and reset $\boldsymbol{P}_k$ to be the better of the two. Then, select the best of all $\boldsymbol{P}_k$ and designate it as $\boldsymbol{P}_{\mathrm{g}}$.

5) Terminate the computation if the number of iterations reaches a preset maximum or if other termination conditions

are met, and output $\boldsymbol{P}_{\mathrm{g}}$ as the result; otherwise, go to 3) and the iteration number increases by one.

Additionally, successively executing Step 2 to Step 5 one time means one 'iteration' of PSO.

B. Linearly Evaluated Fitness Function and its Refinement

Take the nominal operating condition as an example, for a given particle, Fig. 2 schematically indicates the corresponding robust region (confined by the outer irregular dotted line) around the nominal operating point ($\bar{p}_{\mathrm{w1}}$, $\bar{p}_{\mathrm{w2}}$). In other words, (p_{w1}, p_{w2}) could be any point in this region where the damping ratio and frequency shift of the mode satisfy the requirements. However, due to the tremendous difficulties in accurately calculating this region, a round region confined by a circle (thick line), which uses ($\bar{p}_{\mathrm{w1}}$, $\bar{p}_{\mathrm{w2}}$) as its center and is inscribed with the real robust region's contour, is employed as an approximation. In reality, the sizes of two WFs could be fairly different. In such case, $\bar{p}_{\mathrm{w1}}$ will be much larger (or smaller) than $\bar{p}_{\mathrm{w2}}$ when p_{w1} ($\bar{p}_{\mathrm{w1}}$) and p_{w2} ($\bar{p}_{\mathrm{w2}}$) are used in the form of actual values or per-unit values with same basis. Thus, the derived maximum radius will be greatly constrained by the smaller one between $\bar{p}_{\mathrm{w1}}$ and $\bar{p}_{\mathrm{w2}}$, and the round robust region will be very conservative in comparison to the real robust region. In order to avoid such unexpected result, p_{w1} ($\bar{p}_{\mathrm{w1}}$) and p_{w2} ($\bar{p}_{\mathrm{w2}}$) are respectively normalized by their own WF's capacity so that they become comparable even though the WFs' capacities are very different. Thus, the conservativeness of the round robust region induced by the large capacity differences of WFs can be obviously reduced.

Although the round region is comparatively conservative, the robustness of the closed-loop system can be approximately represented by R_{m} which is the radius of the round region. However, acquiring an exact R_{m} is computationally expensive. This paper proposes the use of a linearly approximated but easily obtained R_{m} in each considered operating condition to indicate the quality of the particle. Moreover, if necessary (this matter will be addressed later in this section), more computations will be required to refine R_{m} for a much more accurate R_{m}.

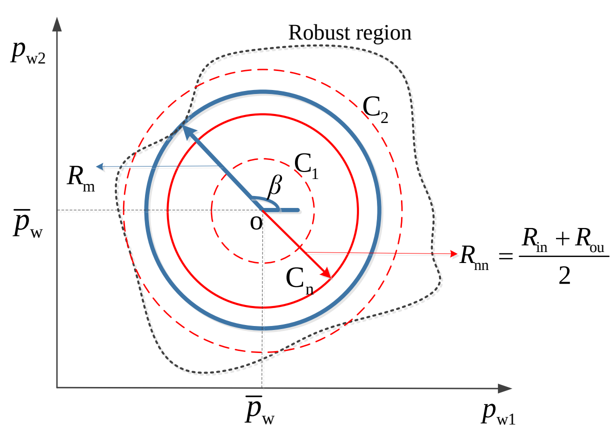

Fig. 2. Robust region and bisection searching

1) Linear prediction of R_{m}

With the open-loop power system and the damping controllers described by the state-space models, the sensitivity of a closed-loop eigenvalue with respect to the wind power at the nominal operating point can be calculated, as follows [21]:

$$\frac{\partial \lambda_i}{\partial p_{\mathrm{w1}}} = \boldsymbol{U}^{-1}(i,:)\begin{bmatrix} \dfrac{\partial \boldsymbol{A}_{\mathrm{o}}}{\partial p_{\mathrm{w1}}} & \dfrac{\partial \boldsymbol{B}_{\mathrm{o}}}{\partial p_{\mathrm{w1}}}\mathbf{C}_{\mathrm{c}} \\ \mathbf{B}_{\mathrm{c}}\dfrac{\partial \boldsymbol{C}_{\mathrm{o}}}{\partial p_{\mathrm{w1}}} & \mathbf{0} \end{bmatrix}\boldsymbol{U}(:,i) \tag{18}$$

where $\boldsymbol{A}_{\mathrm{o}}$, $\boldsymbol{B}_{\mathrm{o}}$, and $\boldsymbol{C}_{\mathrm{o}}$ are the state, input, and output matrices, respectively, of the open-loop power system; $\mathbf{B}_{\mathrm{c}}$ and $\mathbf{C}_{\mathrm{c}}$ are the input and output matrices, respectively, of the synthesized damping controller; and $\boldsymbol{U}(:, i)$ denotes the ith column of the right eigenmatrix $\boldsymbol{U}$ of the closed-loop state matrix. Here, the partial derivatives of $\boldsymbol{A}_{\mathrm{o}}$, $\boldsymbol{B}_{\mathrm{o}}$, and $\boldsymbol{C}_{\mathrm{o}}$ with respect to p_{w1} at the nominal operating point can be calculated irrespective of the controller before the optimization, and then remain unchanged during the optimization. So, deriving $\partial\lambda_i/\partial p_{\mathrm{w1}}$ for a particle requires the following additional calculations: composing $\mathbf{A}_{\mathrm{c}}$ (state matrix of the controller), $\mathbf{B}_{\mathrm{c}}$, $\mathbf{C}_{\mathrm{c}}$, and the closed-loop state matrix based on the particle; computing the right eigenmatrix $\boldsymbol{U}$; and evaluating (18). Moreover, $\partial\lambda_i/\partial p_{\mathrm{w2}}$ can be analogously computed.

The sensitivities of ξ_i with respect to the wind power at the nominal operating point are readily calculated based on the eigenvalues' sensitivities. Therefore, ξ_i will descend fastest along the gradient direction represented by the angle β (Fig. 2), which is derived as follows:

$$\beta = \arctan\left[\left.\frac{\partial \xi_i/\partial p_{\mathrm{w2}}}{\partial \xi_i/\partial p_{\mathrm{w1}}}\right|_{(\bar{p}_{\mathrm{w1}},\bar{p}_{\mathrm{w2}})}\right] \tag{19}$$

The descending speed of ξ_i along this direction is computed as follows:

$$\left.\frac{\partial \xi_i}{\partial l}\right|_{\max} = \sqrt{\left[\left(\partial\xi_i/\partial p_{\mathrm{w1}}\right)^2+\left(\partial\xi_i/\partial p_{\mathrm{w2}}\right)^2\right]\Big|_{(\bar{p}_{\mathrm{w1}},\bar{p}_{\mathrm{w2}})}} \tag{20}$$

Hence, if $\xi_i > \xi_{i\_\mathrm{spec}}$ is the only constraint, the radius R_{m} can be linearly estimated as follows:

$$R_{\mathrm{m}} = \frac{\xi_i - \xi_{i\_\mathrm{spec}}}{\left(\partial\xi_i/\partial l\right)\big|_{\max}} \tag{21}$$

In fact, a predicted R_{m} can be similarly derived for each constraint of (16c). Obviously, the smallest among all predictions is the desired R_{m}.

2) Refining R_{m} by method of bisection

Refining the raw R_{m} derived in the previous subsection will be required for certain particles. Therefore, the bisection method is employed in this paper to improve the accuracy of calculating R_{m}. The general principle of the bisection method is easily understood and briefly presented here based on Fig. 2. All points inside the circle C_1 (inner dashed circle) with the radius equal to R_{in} are assumed to satisfy the constraints (16b) and (16c), while the circle C_2 (outer dashed circle) with radius R_{ou} embraces some points that violate the constraints. Then, a new circle C_{n} with radius $R_{\mathrm{nn}}=(R_{\mathrm{in}}+R_{\mathrm{ou}})/2$ is generated: if the constraints hold over all points along this circle, the circle C_1 will expand to have a radius of R_{nn} (R_{in}=R_{nn}); otherwise, the circle C_2 will shrink to have a radius of R_{nn} (R_{ou}=R_{nn}). Next, based on the refreshed R_{in} and R_{ou}, the circle C_n (R_{nn}) will be regenerated and the expanding or shrinking operation is also repeated. The above procedure will continue until the convergence criterion is met (i.e., R_{in}, R_{nn}, and R_{ou} are very close to each other).

Two specific issues are necessarily addressed for the above searching method. First, N_b points that are uniformly distributed in the circle R_{nn} are evaluated. If the constraints (16b) and (16c) are satisfied for all of these points, then they are simply believed to hold along the whole circle. Second, a point lying in the gradient direction that violates the constraints can be easily found. So, the circle passing through this point is chosen as the starting C_2, and the circle center in Fig. 2 as the starting C_1.

C. Customized PSO Algorithm

The customized PSO algorithm inherits most of the standard PSO algorithm's procedure and operations. However, its unique features are attributed to the following two modifications to the standard PSO.

1) In each iteration, the approximated fitness functions of all particles are first evaluated based on the linear predictions of R_s. All particles are then ordered according to these approximations. The particles ranking in the first few places (with the number of N_c) of the queue are regarded as the high-quality candidates. Thus, if the linearly predicted R_s of these candidates are also larger than zero (indicating the constraints (16b) and (16c) are satisfied at the nominal operating point), the accuracies of their fitness functions will be upgraded by refining R_s.

2) If two particles' fitness functions are both calculated by the linearly predicted R_s (or both by the refined R_s), the one with larger fitness function wins the competition between them; otherwise, the particle with the refined R_s-based fitness function defeats the particle with the fitness function calculated from the linearly predicted R_s.

The flying or evolution process of the particles in PSO is the optimization process of the controllers' parameters. Akin to the general mechanism of the evolutionary algorithms family, PSO also uses the 'best' particle (individual) to lead the evolution direction of the swarm (population). Commonly, the 'best' is determined by comparing individuals' fitness functions. Exactly evaluating the fitness function for each individual ensures the absolute correct selection of the 'best' one, but is fairly time-consuming. Indeed, utilizing the approximated fitness function as an indicator and discarding most of the candidates can save remarkable computing time while causing little adverse impact with respect to determining the actual 'best' individual [14]. So, the customized PSO here extends this idea to estimate the robust region of the WPSS corresponding to each particle. Then, as a result of that estimation, which requires a fairly limited time, the best particle can quite possibly be identified in a significantly reduced computation time because most of the inferior particles have been filtered out by the estimation. Therefore, the customized PSO is expected to perform analogously to the standard PSO to solve (16) but with much better computational efficiency.

V. Simulations And Analysis

In this section, the 10-Machine New England system [22] is amended to incorporate wind power for validating the IGDT-based design method. All computations are carried out with a desktop with a 2.5-GHz Intel Core i5-3210 CPU and 4.00 GB of RAM.

A. Modified New England System

Fig. 3 shows the modified New England system, synchronous generators SG2-SG10 are represented by 4^{th}-order dynamic model [23] and all equipped with AVR of IEEE type II. SG1 which has fairly large inertia time constants represents an external equivalent system. In addition, two WFs with same rated capacity of 1400 MW are attached to Bus-40 and -41 respectively, via short transmission lines. Moreover, the active power load of Bus-16 and -17 are increased by 700 MW, respectively. Here, the WFs are aggregately represented by the DFIG-based WTs. Specifically speaking, 5^{th}-order dynamic model [24] is used; the wind turbine together with the DFIG rotating mass is represented by a two-mass model to take into account the torsional mode associated with the shaft. Additionally, fast stator dynamics of the induction generator are normally neglected. The parameters of the DFIG and the state space equation of the open-loop power system are given in the Appendix. And, loads used in this study are modeled by constant impedances. Moreover, expected power outputs of two WFs are assumed to be identical (700 MW) at all considered operating conditions. SGs and WFs together provide all power supply. Therefore, when the total wind power deviates from the expectation (1400 MW), some SGs are selected to compensate the deviation for the balance between power supply and demand of power system. Here, SG4, SG9 and SG2 commonly and proportionally compensate the deviation according to their own capacities. Specifically, SG4 and SG9 are both supposed to compensate 35% of the deviation while SG2 compensates the residual part.

In addition, eigenvalues of the open-loop system in the nominal operating condition are calculated. There are nine electromechanical oscillation modes including six local modes and three inter-area modes. The traditional phase compensation method is employed to tune six local PSSs for suppressing local power oscillations. Moreover, three inter-area modes shown in Table I are poorly damped. Thus, WPSSs are employed to effectively improve the damping level of this system. Furthermore, based on residue analysis and calculation of participate factors, SG2, SG5 and SG9 are indicated as the most suitable places to install the WPSSs, aiming at the three inter-area modes, respectively. The active power carried by Lines #6-31, #20-34, and #1-2 represents the most effective feedback signals for the WPSSs associated with SG2, SG5, and SG9, respectively. Specifically, WPSSs associated with SG2 and SG5 actually use local signals. It is also tested that the desired damping control effects and robustness can be hardly satisfied when only SG2 and SG5 are employed for installment of PSSs. Hence, another unit SG9 which should use the remote feedback signal is necessarily recruited to cooperate with SG2 and SG5 for damping the inter-area modes. Besides the nominal operating condition, seven more operating conditions which are listed in Table II are considered in this simulation. Particularly, the first four operating conditions in Table II are directly included in the IGDT-based model for the control design while the rest ones are used to verify the effectiveness of the proposed method.

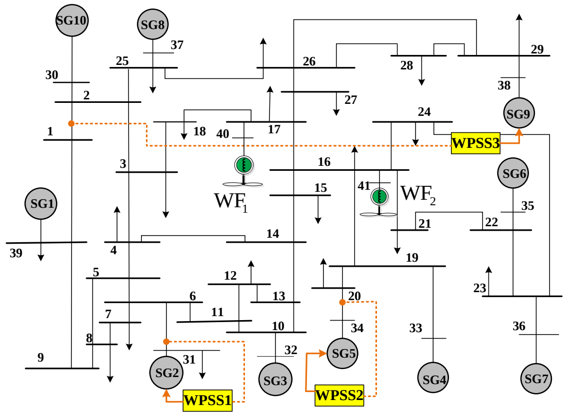

Fig. 3. Modified New England System

B. Tuning WPSS Parameters

In this study, the acceptable damping ratios of three inter-area modes in the first four conditions ($\xi_{i\_spec}^{(1)}$, $\xi_{i\_spec}^{(2)}$, $\xi_{i\_spec}^{(3)}$, $\xi_{i\_spec}^{(4)}$) are set to be 0.09, 0.085, 0.085 and 0.085 respectively; and the allowable frequency drift ratios of three inter-area modes ($\rho_1^{(n)}, \rho_2^{(n)}, \rho_3^{(n)}$) are set to be 5%, 5% and 8%. The weights ($W^{(1)}$, $W^{(2)}$, $W^{(3)}$, $W^{(4)}$) are set to be 1.0, 0.3, 0.3 and 0.3. In addition to the proposed IGDT-based method, the WPSS parameters are also tuned by a comparative robust method that satisfies same damping ratio and frequency excursion ratio requirements as well as optimizes a devised H_∞ index (μ) to enhance the nominal closed-loop system's robustness against model uncertainties [19]. Specifically, based on the small gain theory [25], the H_∞ index (μ) representing system robustness can be obtained by calculating the following equation:

$$\mu = \left\| \left(1 + K(s) P(s)\right)^{-1} \right\|_\infty \tag{22}$$

where $P(s)$ and $K(s)$ are transfer functions of the open-loop system and the feedback control system (WPSSs), respectively, under nominal operating condition; $\|\,\|_\infty$ is the infinite norm of transfer function. It is known that larger μ is desired since it means a better robustness of the system. Accordingly, H_∞ index based optimization model under nominal operating condition is as follows:

$$\max_X \ \mu \tag{23a}$$

$$s.t. \ \left|\omega_i - \omega_{i\_o}\right| / \omega_{i\_o} \le \rho_i \quad i=1, 2, \ldots, N_a \tag{23b}$$

$$\xi_i \ge \xi_{i\_spec} \tag{23c}$$

$$\mathbf{X}_{\min} \le \boldsymbol{X} \le \mathbf{X}_{\max} \tag{23d}$$

In the study, R-WPSSs denote the WPSSs tuned by H_∞ index based method while I-WPSSs represent those obtained by the IGDT-based method. The parameters of the WPSSs are listed in Table III. Specifically, the R_s acquired by solving the optimization problem (16) is 541 MW (here, actual values are used in order to make more practical sense), which means that ($R_m^{(1)}$, $R_m^{(2)}$, $R_m^{(3)}$, $R_m^{(4)}$) are, respectively, 289 MW, 363 MW, 223 MW and 254 MW. Among them, $R_m^{(1)}$ (289 MW) denotes that the required damping control effects will be fulfilled for all points within the circle with a radius of 289 MW (Fig. 2) by I-WPSSs under the nominal operating condition.

TABLE I
INTER-AREA MODES OF OPEN-LOOP POWER SYSTEM

Mode	Eigenvalue (damping ratio)	Generators
1	-0.222±7.304i (3.04%)	SG2, SG9, SG3
2	-0.133±6.878i (1.93%)	SG5, SG9, SG4
3	-0.067±4.278i (1.57%)	SG1, SG5, SG9

TABLE II
MULTIPLE OPERATING CONDITIONS OF MODIFIED NEW ENGLAND SYSTEM

No.	Description
1	Nominal operating condition (expected wind power)
2	Tie-line 15-16 is outage
3	Tie-line 5-6 is outage
4	Tie-line 4-14 is outage
5	Tie-line 9-39 is outage
6	WF1 outputs 905 MW and WF2 outputs 495 MW
7	WF1 outputs 930 MW and WF2 outputs 150 MW
8	Tie-line 9-39 is outage, WF1 outputs 880MW and WF2 outputs 340MW

TABLE III
PARAMETERS OF R-WPSSS AND I-WPSSS

H_∞-based method			
Generator	K	T_1	T_2
SG2	0.2001	0.2349	0.0793
SG5	0.0371	0.3330	0.0638
SG9	0.0190	0.2070	0.1100
IGDT-based method			
SG2	0.1103	0.4982	0.1111
SG5	0.0177	0.5281	0.0654
SG9	0.0145	0.4925	0.1295

C. Effectiveness & Efficiency of Customized PSO Algorithm

In the customized PSO algorithm, the number of particles in the population is set to be 100. Additionally, parameters e, c_1 and c_2 are all set to be 0.2. As mentioned previously, the effectiveness of the customized PSO algorithm is directly associated with the correctness of permuting the particles according to the linearly predicted R_s. Therefore, the 10^{th}, 20^{th}, 30^{th}, 40^{th} and 50^{th} iterations during the PSO search are specifically recorded to demonstrate such permutation. All particles are ordered using the linearly predicted R_s and the refined R_s, respectively, in the selected iterations. Table IV shows the particles ranking in the first five places for these two permutations. Clearly, the permutation based on linear predictions of R_s can capture the high-quality particles with fairly high correctness. This is also obvious evidence that the customized PSO has inherited the searching capabilities of the standard PSO. In particular, the best particles of these iteration population all occur in the first three places of the linear prediction-based permutation, which means that the customized PSO unnecessarily spends a huge amount of time accurately evaluating a large number of particles (refining R_s) to identify the leading (best) one. Thus, in this study, N_c is chosen to be 4. Then, the average time cost of finishing all calculations in one iteration by the customized PSO algorithm is about 5 minutes. In contrast, such time cost will be totally unacceptable (more than one hour) if the fitness functions of all particles are accurately computed. Therefore, the customized PSO algorithm has quite feasible efficiency to deal with the optimization problem for the IGDT-based WPSSs design. Furthermore, the customized PSO algorithm needs about 40 iterations on average to reach a solution.

TABLE IV
VALIDATION OF ACCURACY OF PREDICTION METHOD

Iteration	Refined	Linear Prediction	Accuracy
10	74 87 54 89 17	74 87 54 89 17	100%
20	74 87 54 17 89	74 87 17 54 89	100%
30	87 06 54 42 29	87 06 29 74 42	80%
40	18 42 54 57 87	18 42 57 87 54	100%
50	45 42 35 57 87	76 42 35 57 87	80%

TABLE V
EIGENVALUES OF INTER-AREA MODES IN FIVE OPERATING CONDITIONS

No.	No-Controllers	R-WPSSs	I-WPSSs
1	-0.222±7.304i (3.04%)	-0.824±7.154i (11.44%)	-0.752±7.271i (10.29%)
	-0.133±6.878i (1.93%)	-0.652±6.961i (9.33%)	-0.837±6.683i (12.43%)
	-0.067±4.278i (15.66%)	-0.402±4.285i (9.34%)	-0.504±4.137i (12.09%)
2	-0.184±7.022i (2.62%)	-0.537±7.046i (7.60%)	-0.737±7.109i (10.31%)
	-0.171±6.549i (2.61%)	-0.831±6.569i (12.55%)	-0.963±6.475i (14.72%)
	-0.041±3.985i (1.03%)	-0.375±3.984i (9.37%)	-0.464±3.829i (12.03%)
3	-0.208±7.106i (2.93%)	-0.555±7.015i (7.89%)	-0.739±7.154i (10.27%)
	-0.135±6.870i (1.96%)	-0.884±6.944i (12.63%)	-0.879±6.681i (13.04%)
	-0.068±4.262i (1.59%)	-0.401±4.270i (9.35%)	-0.502±4.122i (12.09%)
4	-0.219±7.289i (2.30%)	-0.858±7.138i (11.93%)	-0.757±7.229i (10.41%)
	-0.131±6.861i (1.91%)	-0.610±6.944i (8.75%)	-0.832±6.685i (12.35%)
	-0.068±4.232i (1.61%)	-0.403±4.236i (9.47%)	-0.499±4.089i (12.11%)
5	-0.199±7.075i (2.81%)	-0.479±7.075i (6.75%)	-0.613±7.149i (8.54%)
	-0.132±6.829i (1.93%)	-0.930±6.762i (13.63%)	-0.951±6.527i (14.42%)
	0.066±3.366i (-1.96%)	-0.331±3.409i (9.64%)	-0.477±3.140i (15.02%)

D. Robustness of WPSSs Designed by the IGDT-Based Method

In this section, eigenvalue analysis and time domain simulations are used to verify the control effects and robustness of I-WPSSs against system parameter changes (i.e. transmission line outages) and wind power variations. Modal analysis for the first five operating conditions (Table II) is carried out and Table V presents the resulted three inter-area modes. Obviously, I-WPSSs can guarantee that all these modes have satisfactory damping ratios and frequency excursion ratios. In contrast, certain modes (e.g. the first mode associated with the emergent operating condition of No. 2) are not with the required damping ratio as R-WPSSs are installed. To further validate the robustness of I-WPSSs against system parameter changes, time-domain simulations are conducted with the emergent operating condition of No. 5. An instantaneous three-phase short-circuit fault occurring at Line #2-3 and lasting for 50ms is applied. The dynamics of the synchronous generators' relative power angles are delineated in Fig. 4. Here, the relative power angle δ_3-δ_9 is the strongest signal with which to observe the first inter-area mode shown in Table I, while δ_5-δ_9 and δ_1-δ_5 are used to observe the second and third inter-area modes, respectively. It is observed in Fig. 4 that I-WPSSs can damp inter-area oscillations more rapidly than R-WPSSs. Above simulation results prove that I-WPSSs have better robustness than R-WPSSs when the system is subjected to transmission line outages.

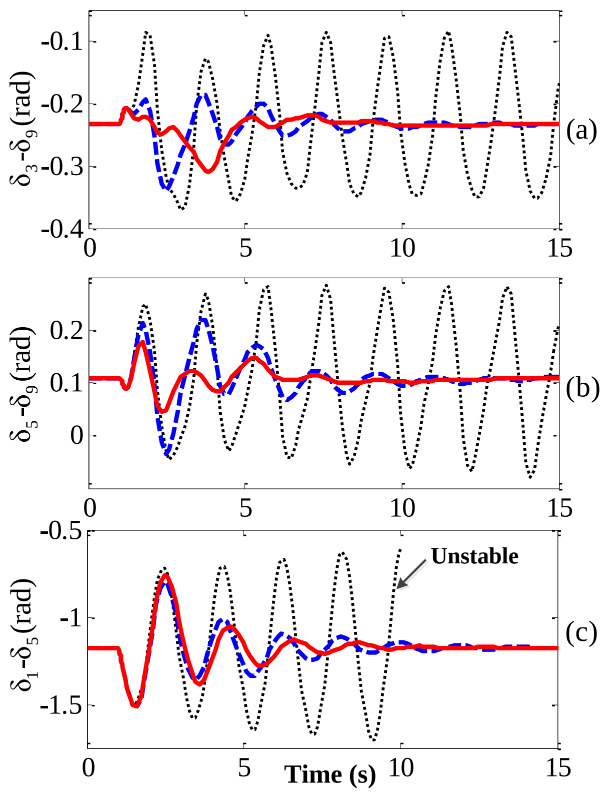

Fig. 4. Relative power angles under No. 5 emergent operation condition (solid line: I-WPSSs; dashed line: R-WPSSs; dotted line: no Controllers)

The nominal and No. 2 emergent operating conditions are selected for validating the robustness of I-WPSSs against wind power variations. First, 5000 points are uniformly sampled within two round regions which have the same center at (700 MW, 700 MW) but with the radiuses of, respectively, 296 MW and 363 MW. Here, each point in the round region corresponds to a wind power output scenario. Then, the eigenvalues of the closed-loop system with I-WPSSs and R-WPSSs, respectively, are calculated for all scenarios. Thus, Figs. 5(a), 5(b), 6(a), and

6(b) depict the distributions of the three inter-area modes in the complex plane, while the probability densities of these modes' damping ratios are illustrated in Figs. 5(c), 5(d), 6(c), and 6(d). Clearly, the I-WPSSs can consistently drive the three inter-area modes to the required area in the complex plane as the WF power outputs vary in the round region. This aligns with another observation for I-WPSSs (Fig. 5 (d)) that the probability densities are equal to zero if the modes' damping ratios are less than 0.9. In contrast, Figs. 5 and 6 both demonstrate that the system controlled by R-WPSSs still has some poorly damped inter-area modes even when the WF power outputs are not beyond the round region. The above results lead to the conclusion that I-WPSSs have better robustness than R-WPSSs against wind power variations.

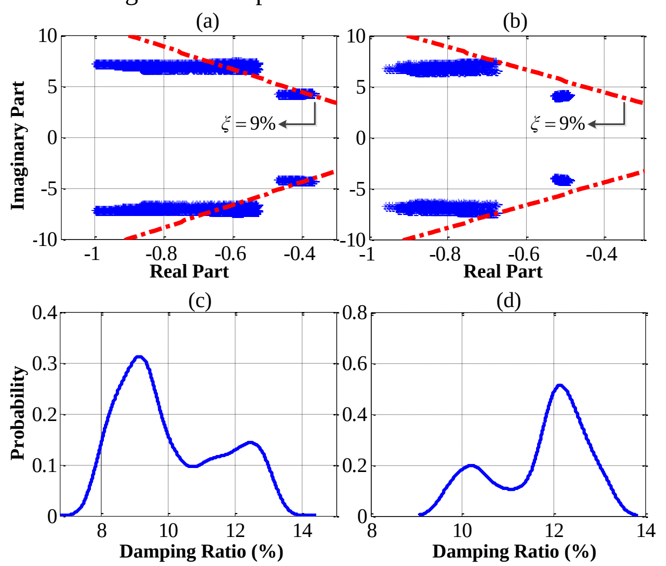

Fig. 5. Locus of inter-area modes and probability densities of damping ratios with varying wind power under nominal operating condition: (a) R-WPSSs; (b) I-WPSSs; (c) R-WPSSs; (d) I-WPSSs.

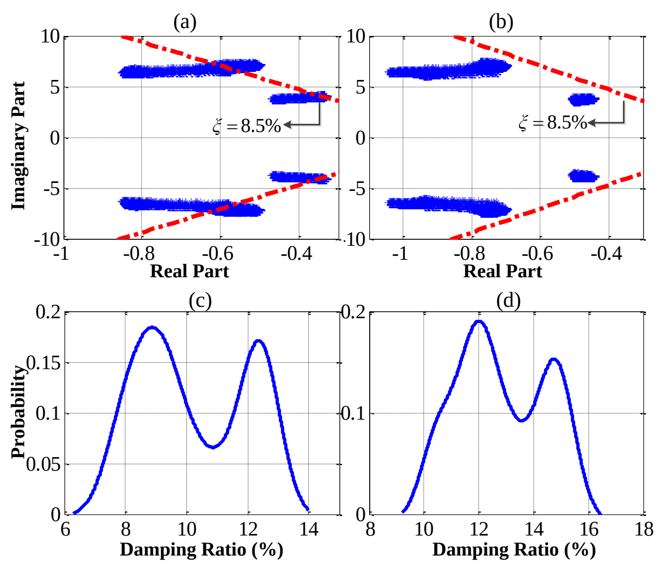

Fig. 6. Locus of inter-area modes and probability densities of damping ratios with varying wind power under No. 2 emergent operating condition: (a) R-WPSSs; (b) I-WPSSs(c); R-WPSSs; (d) I-WPSSs.

Specifically, three wind power scenarios as the power system with nominal configuration are studied: The two WFs both output expected power (700MW) in Scenario 1 (No. 1 operating condition); Scenario 2 (No. 6 operating condition) is corresponding to a point in the boundary of the round region with a radius of 289 MW as mentioned in the previous paragraph; and Scenario 3 (No. 7 operating condition) denotes an extreme point far beyond this round region. Table VI shows the three inter-area modes in the second and third scenarios, and their values in Scenario1 can be found in Table V. It can be observed that I-WPSSs outperform R-WPSSs in all these three scenarios, and the gap between their performances becomes considerable as the WF power outputs deviate further from their nominal values (i.e., the extreme Scenario 3).

TABLE VI
EIGENVALUES OF INTER-AREA MODES IN TWO WIND POWER SCENARIOS

Scenario	No-Controllers	R-WPSSs	I-WPSSs
2	-0.234±7.264i (3.22%)	-0.983±7.188i (13.55%)	-0.913±7.102i (12.75)
	-0.186±6.769i (2.75%)	-0.542±6.765i (7.99%)	-0.717±6.675i (10.68%)
	-0.039±4.301i (0.91%)	-0.367±4.336i (8.43%)	-0.514±4.181i (12.20%)
3	-0.250±7.252i (3.45%)	-1.094±7.159i (15.11%)	-1.088±7.009i (15.34%)
	-0.295±6.324i (4.66%)	-0.558±6.239i (8.91%)	-0.591±6.198i (9.49%)
	0.020±4.204i (-0.48%)	-0.325±4.297i (7.5%)	-0.590±4.102i (14.24%)

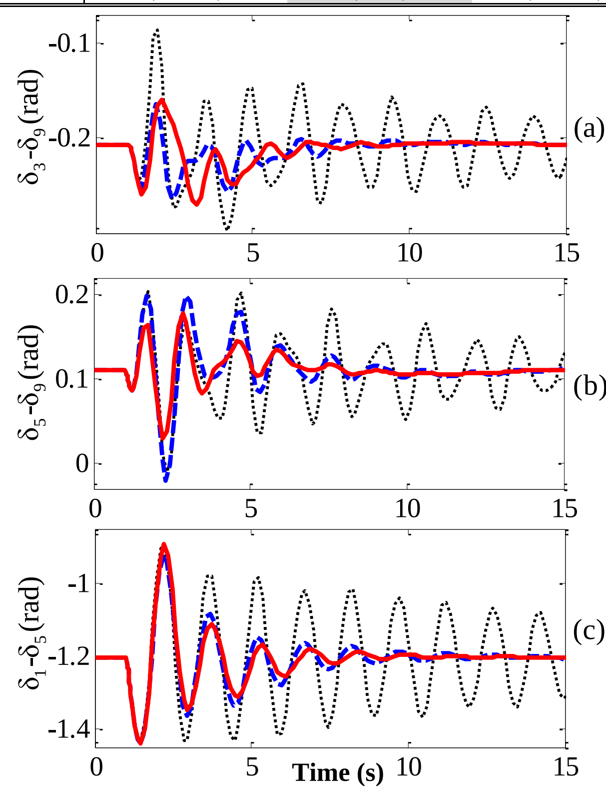

Fig. 7. Relative power angles under Scenario 1 (solid line: I-WPSSs; dashed line: R-WPSSs; dotted line: no Controllers)

Time domain simulations with the three wind power scenarios are carried out in Figs. (7)-(9). The dynamics dominated by these modes again confirm the satisfactory robustness of I-WPSSs, which rapidly annihilate the inter-area oscillations in all three scenarios. Furthermore, the R-WPSSs also acceptably damp the inter-area oscillations in the first and second scenarios. Thus, the obvious degeneration of R-WPSS control effects in the third scenarios indicates that the robustness gained by only using the system's information at the nominal point is locally effective but unable to withstand model uncertainties varying over a large region. This justifies the IGDT-based design method, which uses the direct and explicit robustness index as the optimization objective.

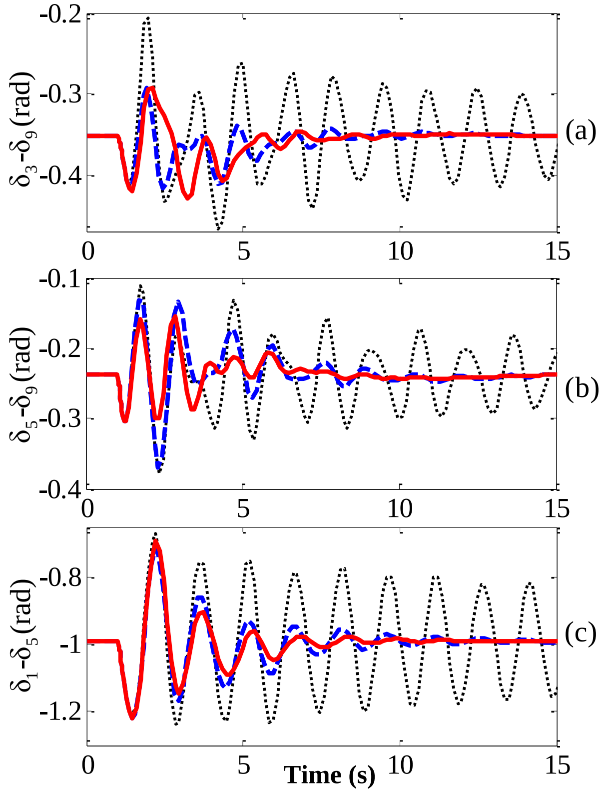

Fig. 8. Relative power angles under Scenario 2 (solid line: I-WPSSs; dashed line: R-WPSSs; dotted line: no Controllers)

E. Comparison of Control Efforts Between I-WPSSs and R-WPSSs

In this subsection, the superior performance of I-WPSSs with respect to R-WPSSs will be further justified by comparing their control efforts. Particularly, this paper utilizes the integrated map under the envelop of a controller' output curve over the simulation time to simply indicate the control effort of this controller. Therefore, a simple comparison is conducted as with the operating condition of No. 8 in Table II. The time domain simulation is performed with the same disturbance used previously and the control efforts of the damping controllers are computed. Since there are three individual WPSSs installed with SG2, SG5 and SG9, respectively, their control efforts are correspondingly marked by V_{ss1}, V_{ss2} and V_{ss3}. Then, Fig. 10(a) compares the control efforts when the two compared design methods are respectively employed to tuning the WPSSs. It is seen that the values of V_{ss1} derived with the two design methods are quite close. In fact, analogous situation is also observed in V_{ss2} and V_{ss3}. Moreover, the values of these control efforts can also be found in Appendix. All these results actually tell that I-WPSSs and R-WPSSs have very close control efforts. However, from the comparisons of damping ratios of the three inter-area modes in Fig. 10(b) and dynamic curves of the relative power angle in Fig. 11, it is also observed that I-WPSSs has better control performance than R-WPSSs. Consequently, the above comparison results are the direct evidence that I-WPSSs do not depend on unfair use of control efforts to win the competition with R-WPSSs, and its superior performance is derived through appropriately tuning the parameters by the proposed IGDT-based optimization method.

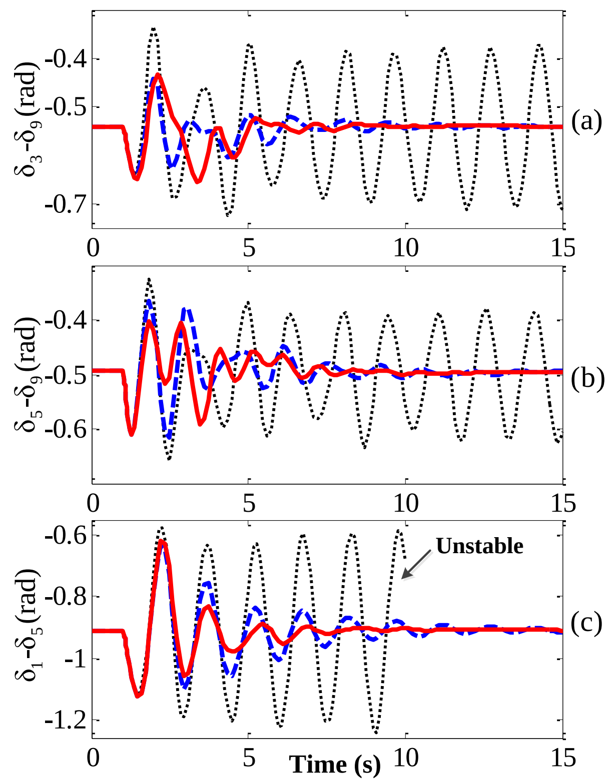

Fig. 9. Relative power angles under Scenario 3 (solid line: I-WPSSs; dashed line: R-WPSSs; dotted line: no Controllers)

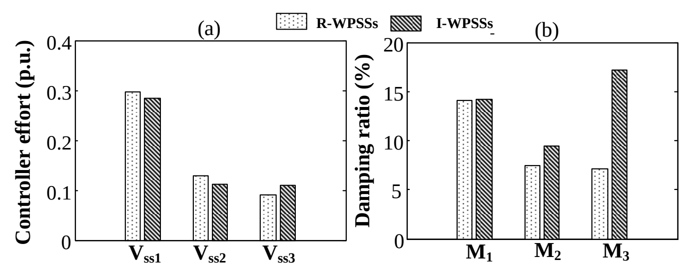

Fig. 10. (a) Control efforts of R-WPSSs and I-WPSSs; (b) Damping ratios of three inter-are modes with R-WPSSs and I-WPSSs (M1: first inter-are mode; M2: second inter-are mode; M3: third inter-are mode).

VI. Conclusion

In this paper, IGDT is proposed to deal with the uncertainties of WF steady-state power outputs and to design the robust WPSSs to suppress inter-area oscillations with consideration of WF power outputs variations and transmission line outages. Theoretically, in the normal or emergent conditions, WPSSs can fulfill the requirements to damp inter-area oscillations if the WF power outputs vary in a feasible range. Thus, by optimizing the WPSS parameters to maximize this feasible range via a formulated optimization problem constructed based on IGDT, robust WPSSs can be derived. Furthermore, the linear prediction technique of eigenvalues is employed to produce a customized PSO algorithm that efficiently finds a satisfactory optimization solution. Simulations of the modified New England system confirm the effectiveness and robustness of the WPSSs designed using IGDT.

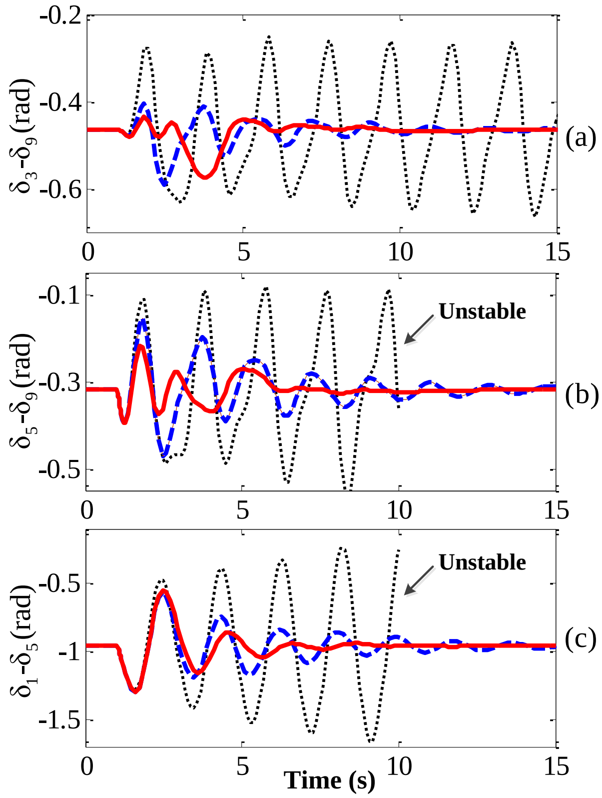

Fig. 11. Relative power angles under No. 8 operating condition (solid line: I-WPSSs; dashed line: R-WPSSs; dotted line: no Controllers)

Appendix

A. Parameters of DIFG Model

Parameters of DFIG-based WT [14]: WT radius = 35 m; Gear box ratio = 74; R_s = 0.00488; R_r = 0.00549; X_s = 0.09241; X_m = 3.95279; and H = 3.5s.

B. State Space Equation of Open-loop System

The sate space equation of open-loop power system is represented by equation (24), and corresponding state vector, input vector and output vector are as follows:

$$\begin{cases} \dot{\mathbf{X}}_o = \mathbf{A}_o\mathbf{X}_o + \mathbf{B}_o\mathbf{u}_c \\ \mathbf{Y}_o = \mathbf{C}_o\mathbf{X}_o \end{cases} \tag{24}$$

where $\mathbf{X}_o$ is the state vector of the open loop system, and $\mathbf{X}_0$ is consisted of the state variables of δ, ω, e'_d, e'_q, v_m, v_{r1}, v_{r2}, v_f, θ_{tw}, ω_t, ω_r, e_{wd}, and e_{wq}: δ is the rotor angle of synchronous generator (SG); ω is the rotor speed of SG; e' is the transient voltage of SG; 'd' or 'q' subscripts indicate that the relevant variables are d-axis or q-axis components, respectively; v_m, v_{r1}, v_{r2}, and v_f are the state variables associated with AVR of IEEE Type II; θ_{tw} is the shaft twist angle of wind turbine; ω_t and ω_r are the rotor speeds of wind turbine and DFIG, respectively; e_w is the internally generated voltage of DFIG; $\mathbf{u}_c$ is the control input vector of the open-loop power system which is consisted of supplementary excitation signals of the SGs engaging in the damping control; $\mathbf{Y}_o$ is the output vector which is selected in this paper to be with signals of active power carried by transmission lines; $\mathbf{A}_o$, $\mathbf{B}_o$ and $\mathbf{C}_o$ are the state, input and output matrices, respectively, of the open-loop power system.

C. Three Inter-are Modes of Closed-loop System under No. 8 Operating Condition

Table I
Eigenvalues of Inter-Area Modes under No. 8 Operating Condition

Condition	No-Controllers	R-WPSSs	I-WPSSs
No.8	-0.202±6.995i (2.88%)	-0.983±6.890i (14.10%)	-0.968±6.746i (14.21%)
	-0.226±6.591i (3.43%)	-0.488±6.567i (7.41%)	-0.625±6.546i (9.50%)
	0.142±3.376i (-4.20%)	-0.245±3.440i (7.09%)	-0.546±3.137i (17.13%)

D. Control Efforts of R-WPSSs and I-WPSSs under No. 8 Operating Condition

Table II
Control Efforts of R-WPSSs and I-WPSSs under No. 8 Operating Condition

Controllers	R-WPSSs (p.u.)	I-WPSSs (p.u.)
1	0.2965	0.2839
2	0.1289	0.1126
3	0.0904	0.1089

References

[1] J. G. Slootweg and W. L. Kling, "The impact of large scale wind power generation on power system oscillations," *Elect. Power Syst. Res.*, vol. 67, no.1, pp. 9-20, Oct. 2003.

[2] A. E. Leon, "Integration of DFIG-based wind farms into series-compensated transmission systems," *IEEE Trans. Sustain. Energy*, vol. 7, no. 2, pp. 451-460, Apr. 2016.

[3] D. Gautam, V. Vittal, and T. Harbour, "Impact of increased penetration of DFIG-based wind turbine generators on transient and small-signal stability of power systems," *IEEE Trans. Power Syst.*, vol. 24, no. 3, pp. 1426-1434, Aug. 2009.

[4] Y. Liu, J. R. Gracia, T. J. King, and Y. L. Liu, "Frequency regulation and oscillation damping contributions of variable-speed wind generators in the U.S. Eastern Interconnection (EI)," *IEEE Trans. Sustain. Energy*, vol. 6, no. 3, pp. 951-958, Jul. 2015.

[5] W. Du, X. Chen, and H. F. Wang, "Impact of dynamic interactions introduced by the DFIGs on power system electromechanical oscillation modes," *IEEE Trans. Power Syst.*, in press.

[6] F. M. Hughes, O. Anaya-Lara, N. Jenkins, and G. Strbac, "A power system stabilizer for DFIG-based wind generation," *IEEE Trans. Power Syst.*, vol. 21, no. 2, pp. 763-772, May. 2006.

[7] L. Fan, H. Yin, and Z. Miao, "On active/reactive power modulation of DFIG-based wind generation for interarea oscillation damping," *IEEE Trans. Energy Convers.*, vol. 26, no. 2, pp. 513-521, Jun. 2011.

[8] M. Singh, A. J. Allen, E. Muljadi, V. Gevorgian, Y. Zhang, and S. Santoso, "Inter-area oscillation damping controls for wind power plants," *IEEE Trans. Sustain. Energy*, vol. 6, no. 3, pp. 967-975, Jul. 2015.

[9] K. Elkington and M. Ghandhari, "Non-linear power oscillation damping controllers for doubly fed induction generator in wind farms," *IET Renew. Power Gener.*, vol. 7, no. 2, pp. 172-179, Mar. 2013.

[10] J. Morato, T. Knuppel, and J. Ostergaard, "Residue-based evaluation of the use of wind power plants with full converter wind turbines for power oscillation damping control," *IEEE Trans. Sustain. Energy*, vol. 5, no. 1, pp. 82-89, Aug. 2014.

[11] Y. Mishra, S. Mishra, F. Li, Z. Dong, and R. Bansal, "Small-signal stability analysis of a DFIG-based wind power system under different modes of operation," *IEEE Trans. Energy Convers*., vol. 24, pp. 972–982, Dec. 2009.

[12] T. Surinkaew and I. Ngamroo, "Coordinated robust control of DFIG wind turbine and PSS for stabilization of power oscillations considering system uncertainties," *IEEE Trans. Sustain. Energy*, vol. 5, no. 3, pp. 823-833, Jul. 2014.

[13] H. Huang and C. Y. Chung, "Coordinated damping control design for DFIG-based wind generation considering power output variation," *IEEE Trans. Power Syst*., vol. 27, no. 4, pp. 1916-1925, Nov. 2012.

[14] D. P. Ke and C. Y. Chung, "Design of probabilistically-robust wide-area power system stabilizers to suppress inter-are oscillations of wind integrated power systems," *IEEE Trans. Power Syst*., vol. 31, no. 6, pp. 4297-4309, Jan. 2016.

[15] Y. B. Haim, *Info-Gap Decision Theory*, 2nd ed. San Diego, CA: Academic, 2006.

[16] A. Rabiee, A. Soroudi, and A. Keane, "Information gap decision theory based OPF with HVDC connected wind farms," *IEEE Trans. Power Syst*., vol. 30, no. 6, pp. 3396–3406, Nov. 2015.

[17] A. Soroudi and M. Ehsan, "IGDT based robust decision making tool for DNOs in load procurement under severe uncertainty," *IEEE Trans. Smart Grid*, vol. 4, no. 2, pp. 886–895, Jun. 2013.

[18] B. Mohammadi-Ivatloo, H. Zareipour, N. Amjady, and M. Ehsan, "Application of information-gap decision theory to risk-constrained self-scheduling of GenCos," *IEEE Trans. Power Syst*., vol. 28, no. 2, pp. 1093–1102, May 2012.

[19] M. Green and D. J. N. Limebeer, *Linear Robust Control*. New York: Dover Publications, 2012.

[20] J. Kennedy and R. Eberhart, "Particles swarm optimization," *IEEE Int. Conf. Neural Network*, vol. 15, pp. 1942-1948, Perth, Australia, Nov. 1995.

[21] F. L. Pagola, I. J. Perez-Arriaga, and G. C. Verghese, "On sensitivities, residues and participation: application to oscillatory stability analysis and control", *IEEE Trans. Power Syst.*, vol. 4, no. 1, pp. 278-285, Feb. 1989.

[22] K. R. Padiyar, *Power System Dynamic Stability and Control*. Singapore: Wiley, 1996.

[23] F.Milano, *Power System Analysis Toolbox Version 2.1.8*. Albacete, Spain: Universidad de Castilla-La Mancha, 2013.

[24] O. Anaya-Lara, N. Jenkins, J. Ekanayake, P. Cartwright, and M. Hughes, *Wind Energy Generation—Modelling and Control*, Wiley, 2009.

[25] S. Skoqestad and I. Postlethwaite, *Multiple Feedback Control: Analysis and Design*. Hoboken, NJ, USA: Wiley, 2005.

Deping Ke received the B.S degree in Electrical Engineering in 2005 from Huazhong University of Science and Technology, Wuhan, China, and the Ph.D. degree in Electrical Engineering from The Hong Kong Polytechnic University in 2012. Currently, he is an Associate Professor with the School of Electrical Engineering, Wuhan University, China. His research interests are in power system dynamics and control, and economic operation of power systems.

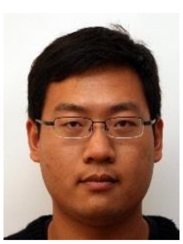

Feifan Shen received the B.Eng degree in Electrical Engineering and Automation, Hohai University, Nanjing, China, in 2015 and the M.Eng degree from Department of Electrical Engineering, Wuhan University, China, in 2017. Currently, he is pursing the Ph.D. degree in the Centre of Electric Power and Energy, Department of Electrical Engineering, Technical University of Denmark, Kgs. Lyngby, Denmark.

C. Y. Chung (M'01–SM'07–F'16) received the Ph.D. degree in electrical engineering from The Hong Kong Polytechnic University in 1999. He is currently a Professor and the SaskPower Chair in Power Systems Engineering in the Department of Electrical and Computer Engineering at the University of Saskatchewan, Saskatoon, SK, Canada. His research interests include power system stability/control, planning and operation, computational intelligence applications, power markets, and electric vehicle charging. Dr. Chung is an Editor of the IEEE TRANSACTIONS ON SUSTAINABLE ENERGY and an Editorial Board Member of IET GENERATION, TRANSMISSION & DISTRIBUTION. He is also a Member-at-Large (Smart Grid) of IEEE PES Governing Board and the IEEE PES Region 10 North Chapter Representative.

Chen Zhang (S'16) received the B.S degree in Electrical Engineering in 2014 from Wuhan University, Wuhan, China. Currently, he is pursuing the Ph.D. degree in the School of Electrical Engineering, Wuhan University. At present, he is also funded by Chinese Scholarship Council (CSC) as a joint Ph. D. student in the Department of Electrical Engineering and Computer Science, Case Western Reserve University, Cleveland, Ohio, USA.

His research interests are in power system stability and control, wind power, and direct load control.

Jian Xu (M'08) received the Ph.D. degree in electrical engineering from the Wuhan in 2007. He joined Wuhan University as a Lecturer in 2007. Since 2015, he has been a Professor of the School of Electrical Engineering at Wuhan University. During 2013–2014, he was a visiting scholar at the Energy Systems Innovation Center, Washington State University, Pullman, WA, USA.

His research interests include power system stability and control.

Yuanzhang Sun(M'99-SM'01) received the B.S. degree from Wuhan University of Hydro and Electrical Engineering, Wuhan, China, in 1987, the M.S. degree from the Electric Power Research Institute(EPRI), Beijing, China, in 1982, and the Ph.D. degree in electrical engineering from Tsinghua University, Beijing, in 1988.

Currently, he is a Professor of the School of Electrical Engineering at Wuhan University, and a Chair Professor of the Department of Electrical Engineering and Vice Director of the State Key Lab of Power System Control and Simulation at Tsinghua University. His main research interests are in the areas of power system dynamics and control, wind power, voltage stability and control, and reliability.